Materials Research, Vol. 6, No. 4, 605-613, 2003.

Microstructural Path of Recrystallization in a Commercial Al-Mn-Fe-Si (AA3003) Alloy

Paulo Rangel Rios[a]*, *Angelo Fernando Padilha*[b]

[a] *Universidade Federal Fluminense*
Av. dos Trabalhadores, 420, 27255-125 Volta Redonda - RJ, Brazil
[b] *Universidade de São Paulo, Departamento de Eng. Metalúrgica e de Materiais da EPUSP*
Av. Prof. Mello Moraes, 2463, 05508-900 São Paulo - SP, Brazil

Received: April 25, 2003; Revised: August 18, 2003

The phenomenological analysis of recrystallization data is described. The concept of microstructural path is briefly introduced as well as some of its relevant equations. The correct equation for the impingement compensated chord length is introduced and used here for the first time. The theory is then applied to data from the recrystallization of a commercial Al-Mn-Fe-Si (AA3003) alloy. It is concluded that nucleation is site saturated and that the grain boundary velocity decreases with time. The analysis also shows that the shape of the recrystallized regions significantly deviates from spherical as the reaction progresses, probably because of the boundary/precipitates interaction.

Keywords: *microstructure, kinetics, nucleation, growth, recrystallization, aluminum alloys*

1. Introduction

Plastic deformation of a metal results in an increase of its free energy. Point, line and planar defects contribute to this "stored" energy. Heating to a convenient temperature leads to recovery and recrystallization. These are among the most important issues of Physical Metallurgy and have been the subject of many publications in the last century[1-3].

During recrystallization new, strain-free grains, nucleate and grow restoring the microstructure that existed before plastic deformation. Possible nucleation mechanisms are: bulge or strain induced grain boundary (present in the microstructure before deformation) migration[4-6], subgrain growth[7,8] and subgrain coalescence[9-12]. Nucleation in recrystallization does not occur because of fluctuations as in the classical nucleation theory. The driving force for growth is the free energy difference between the recrystallized and deformed regions. The interface of the recrystallized grains migrates with a velocity linearly related to the driving force[3]:

$$G = MP \tag{1}$$

where G is the interface velocity, P is the driving force and the constant of proportionality M is the grain boundary mobility.

Recrystallization is a thermally activated nucleation and growth reaction. Recrystallization progress is followed by quantitative metallography. The volume fraction of recrystallized phase, V_V, the interfacial area per unit of volume between recrystallized and deformed regions, S_V, and, less often, interfacial area per unit of volume between recrystallized and recrystallized regions, S_{VR}, are measured.

Geometric and kinetic models can be helpful to find out the time dependence of the nucleation, the spatial distribution of the recrystallization nuclei and the interface migration rate. Crystallographic texture, solutes and second-phase particles can significantly complicate the analysis.

The phenomenological theory introduced by Johnson and Mehl[13], Avrami[14-16] and Kolmogorov[17], the JMAK theory, is almost always employed. This theory supplies several expressions for the volume fraction recrystallized as a function of time for different nucleation rates. It assumes a random distribution of nuclei and a constant interface velocity. It only needs measurements of volume fraction of recrystallized grains, V_V. However, the JMAK theory

*e-mail: prrios@metal.eeimvr.uff.br, padilha@usp.br

is not enough to describe recrystallization. Several authors proposed adjustments to extend it to more complex cases. The microstructural path, proposed by DeHoff[18], is an important idea for the analysis of recrystallization kinetics. He proposed that recrystallization follows a path in the S_V *vs.* V_V space. The microstructural path method, MPM, has been subsequently developed and extensively employed, notably by Vandermeer and coworkers in many excellent papers[19-21].

This work briefly describes the microstructural path method and applies it to an aluminum AA3003 alloy subjected to different degrees of deformation before recrystallization. It is worthy of note that JMAK theory can be applied to various nucleation and growth phase transformations, such as crystallization of glass[22], recrystallization and eutectoid transformations.

The AA3003 alloy is one of the oldest and most used aluminum alloys and therefore the study of its recrystallization behavior is relevant. It has a mechanical resistance that fills the gap between the commercially pure aluminum and the high strength precipitation hardened aluminum alloys. Adding manganese to the commercially pure aluminum increases its mechanical resistance at the expense of a small decrease in ductility. The corrosion resistance of the AA3003 alloy is even better than that of the commercially pure aluminum. The study of this alloy is also interesting because the presence of incoherent Al_6(Mn,Fe) and α-Al(Mn,Fe)Si particles results in a different deformation and recrystallization behavior[23-26]. Particles cause an inhomogeneous deformation because in the volume around them there is a high density of geometrically necessary dislocations. Also, it is well-known that particles weaken the recrystallization texture. Besides, the particles significantly restrict grain growth in this alloy.

2. Phenomenological Analysis of Recrystallization

2.1. The JMAK theory for site-saturated reactions

The first step of the theory is to model the nucleation and growth of the individual recrystallized grains as if they grew independently of one another. The total recrystallized volume obtained in this way is obviously much larger than the real recrystallized volume. It receives the special name of "extended volume", V_{ex}. This quantity is usually divided by the total volume resulting in an "extended volume fraction", V_{Vex}. The extended volume fraction can be larger than one and, except at the earliest stages before impingement begins, is always larger than the real volume fraction.

To calculate V_{Vex} it is necessary to define the nucleation rate, shape and growth rate of the extended grains. The simplest assumption about nucleation is that of site saturation. This means that at $t = 0$ a fixed number of grains per unit volume, N_V, starts to grow and no new grains appear after that.

The simplest assumption about the shape of an extended grain is that it is spherical so the extended volume fraction can be written as:

$$V_{Vex} = N_V\left(\frac{4\pi R_{ex}^3}{3}\right) \tag{2}$$

It remains to define the growth rate of the extended grains and integrate it to obtain R_{ex}. The interface migration rate is directly proportional to the driving force. If the latter remains constant it is natural to expect that the growth rate also remains constant during recrystallization:

$$\frac{dR_{ex}}{dt} = G_0 \tag{3}$$

where G_0 is independent of time or volume fraction recrystallized. It is important to stress that Eq. 3 is an *assumption* of the model. This assumption will be better or worse depending on whether the interface migration rate remains constant. The extended volume can then be written as:

$$V_{Vex} = \frac{4\pi N_V G_0^3 t^3}{3} \tag{4}$$

The second step of the JMAK theory consists in relating the extended volume fraction to the real volume fraction. This can be done with a geometric relationship, mathematically exact for a spatially random distribution of nuclei[13-17]:

$$V_V = 1 - \exp(-V_{Vex}) \tag{5}$$

Equation 5 relates the observed volume fraction transformed in real space, V_V, to the extended volume fraction, V_{Vex}, obtained in extended space. Combining Eqs. 4 and 5 results in the well-known equation:

$$V_V = 1 - \exp\left(-\frac{4\pi N_V G_0^3 t^3}{3}\right) \tag{6}$$

2.2. Modifications of the JMAK theory

Equation 6 is rarely observed to fit recrystallization kinetics. The time exponent obtained from recrystallization data is usually smaller than three, when such a fit is possible at all.

Equation 6 can be modified in several ways. It is possible, for example, to use a constant nucleation rate in-

stead of site-saturation nucleation. It is also possible to consider preferential nucleation sites such as random lines or planes[27]. Fortunately, site-saturated recrystallization has been often observed[19-21]. On the other hand, interface velocity, often decreases with time or volume fraction recrystallized[28,29]. Therefore most models concentrate in the interface velocity.

The most common expression for interface velocity, G, always used by Vandermeer and coworkers[19-21], is:

$$G = \frac{dR_{ex}}{dt} = \frac{G_k}{t^k} \tag{7}$$

where G_k and k are adjustable parameters. For $0 < k < 1$, Eq. 7 can be integrated resulting in:

$$V_{Vex} = \left(\frac{4\pi N_V G_k^3}{3} \right) t^{3(1-k)} \tag{8}$$

or

$$V_V = 1 - \exp\left(- \frac{4\pi N_V G_0^3 t^{3(1-k)}}{3} \right) \tag{9}$$

In this way the original form of Eq. 4 is preserved but with a time exponent less than three. This is the main justification for using an expression of the form of Eq. 7. Speich and Fisher[29] proposed different method for k equal to one.

Equation 9 is often written as:

$$V_V = 1 - \exp\left(- Kt^n\right) \tag{10a}$$

or in logarithmic form:

$$\ln\ln\left(\frac{1}{1-V_V} \right) = \ln K + n \ln t \tag{10b}$$

Because the lack of fundamental justification for Eq. 9, there have been many tries to model the grain boundary velocity considering the physical reasons that lead to its decrease. Two main reasons have been invoked:

a) Concurrent recovery: this would result in a decrease in the stored energy during recrystallization and a consequent decrease in grain boundary velocity.
b) Existence of deformation gradients in the microstructure: the idea here is that the recrystallization would begin in regions of higher stored region and grow into regions of progressively lower stored energy. This would cause a decrease in grain boundary velocity.

Stüwe, Padilha and Siciliano[30] is an example of a model that takes recovery into account whereas Rios[31] is an example of a deformation gradient model.

2.3. Microstructural path of site-saturated recrystallization

When one examines Eq. 9 more closely a difficulty arises. For example, consider the following equation, adapted from the result obtained by Vandemeer and Rath[28] for the recrystallization of an iron single crystal:

$$V_{Vex} = Kt^{0.64} \tag{11}$$

where K is a constant. When Eq. 11 is compared with Eq. 9 one cannot say that k = -0.38 unless one is sure the nucleation is site-saturated. This shows the main drawback of JMAK analysis: it is normally not possible to separate nucleation rate from growth rate.

DeHoff's idea[18] of microstructural path introduced another fundamental quantity besides V_V, the interfacial area between the recrystallized grains and the deformed matrix, S_V. From the analysis of the microstructural path in the (V_V, S_V) space one is able to obtain information about the nucleation.

The fundamental relationship from DeHoff's work is:

$$S_{Vex} = \frac{S_V}{1 - V_V} \tag{12}$$

where S_{Vex} is the extended interfacial area per unit of volume. S_{Vex} is defined in a way similar to V_{Vex}. It is the total interfacial area per unit of volume of the grains considering that they could grow independently of one another. For site-saturated reactions and spherical grains in extended space:

$$S_{Vex} = 4\pi R_{ex}^2 N_V \tag{13}$$

Using Eq. 2 and 13 it can be shown that:

$$S_{Vex} = 3\left(\frac{4\pi N_V}{3} \right)^{1/3} (V_{Vex})^{2/3} \tag{14}$$

This is the microstructural path of site-saturated reactions in extended space. It can be transformed into real space quantities with the help of Eq. 5 and 12:

$$S_V = 3\left(\frac{4\pi N_V}{3} \right)^{1/3} (1 - X_V) \left[\ln\left(\frac{1}{1 - X_V} \right) \right]^{\frac{2}{3}} \tag{15}$$

If the recrystallization is site-saturated it follows the microstructural path described by Eq. 15. If Eq. 15 is obeyed then Eq. 11 results in k = -0.38. It is important to point out that Eq. 15 is always valid for site-saturation regardless of the time dependence of the interface velocity.

2.4. Measures of the interface velocity

Another key issue in analyzing recrystallization is to determine the interface velocity. In section 2.3 it was shown how this can be done directly from Eq. 11 for site saturation reactions. Unfortunately that method depends on the assumption that the interface velocity has the particular form given by Eq. 8.

The first method used to estimate velocity was the method of the maximum grain size. This method consists in measuring the size of the largest recrystallized grain that one could find in the plane of polish. It can only be used in the early stages before significant impingement occurs. This older method has been replaced by a method proposed by Cahn and Hagel[32]. These authors showed that the interfacial migration rate, G_{CH}, is given by:

$$G_{CH} = \frac{1}{S_V}\frac{dV_V}{dt} \tag{16}$$

This expression provides a convenient method for obtaining G_{CH} from experimentally measured values of S_V and V_V. For spherical grains in extended space, Eqs. 12 and 16 give:

$$G_{CH} = \frac{dR_{ex}}{dt} \tag{17}$$

Cahn and Hagel[32] has the disadvantage of needing to determine a derivative from experimental data. This can be difficult specially if one considers the usually large scatter present in recrystallization data. In recent papers, Vandermeer and Jensen[20,21] proposed a new quantity: the impingement-compensated chord length, λ_{ex}, to study the growth of the recrystallized grains. Rios and Padilha[33] corrected the mistake in their original equation and proposed a new one:

$$\lambda_{ex} = \frac{-4(1-V_V)\ln(1-V_V)}{S_V} \tag{18}$$

This expression can be useful to analyze growth rate during recrystallization. Its main advantage is that it can be easily determined from quantities measured from the plane of polish without the need to measure time derivatives. However it is not a growth rate but the integral of a growth rate, so the growth rate has to be inferred from the slope of a λ_{ex} against time plot. Also it is implicitly assumed in the derivation of Eq. 18 that all regions are randomly distributed.

2.5. Grain shape considerations for site-saturated recrystallization

Yamamoto, Sakuma and Rios[34] noticed that the shape of the grains in real space, because of impingement, is different from the shape of the grains in extended space. If, in extended space, there are N_V grains per unit of volume of area S_E and volume v_E:

$$\frac{s_{ex}}{(v_{ex})^{\frac{2}{3}}} = A_{ex} \tag{19}$$

where A_{ex} is a shape factor. Since there is no impingement in extended space the grains have a constant shape and A_{ex} remains the same throughout the reaction. For site-saturation N_V is constant and all grains have the same size so:

$$\frac{S_{Vex}}{(V_{Vex})^{\frac{2}{3}}} = A_{ex}(N_V)^{\frac{1}{3}} \tag{20}$$

In real space, an "average" grain of area s and volume v gives:

$$\frac{s}{(v)^{\frac{2}{3}}} = A \tag{21}$$

where A is a shape factor. Eq. 21 results in:

$$\frac{S_{VT}}{(V_V)^{\frac{2}{3}}} = A(N_V)^{\frac{1}{3}} \tag{22}$$

where

$$S_{VT} = S_V + 2S_{VR} \tag{23}$$

S_{VT} is the total interface area per unit of volume, S_{VR} is the interface area between the recrystallized regions per unit of volume. Remembering that for site-saturated reactions the number of grains per unit of volume in extended and real space is identical, one has:

$$S_{Vex} = \alpha\left(\frac{V_{Vex}}{V_V}\right)^{\frac{2}{3}} S_V^T \tag{24}$$

where $\alpha = A_{ex}/A$ is a shape factor.

Equation 24 is an alternative way of presenting the data for the microstructural path analysis of site-saturated reactions. Its advantages are that data from reactions with different values of N_V can be plotted together and, except for α, all quantities in Eq. 24 can be easily measured. Equation 24 needs both S_V and S_{VR}. In the beginning of the reac-

tion, before significant impingement (say for $V_V < 0.3$), the shape of the growing regions in real space is likely to remain constant. As impingement starts it is reasonable to expect the growing regions will change their shape. Notwithstanding, if the growing regions remain equiaxed this change in shape probably results in a small change in the shape factor, α. For example, if the grains are spherical at the beginning of the reaction but become tetrakaidecahedra towards its end then *A* will increase from 4.8 to 5.3. Since the sphere has the minimum area for a given volume one might expect α to be smaller than the unity.

3. Experimental Materials and Methods

The content of the alloying elements in the AA3003 aluminum alloy was, in wt.%: 0.90 Mn; 0.63% Fe; 0.19% Si; 0.14% Cu; 0.014%Ti, and less than 0.1% of other elements. Specimens from the as received hot rolled 6 mm thick plates were stabilized at 673 K for 8 h (28800 s) followed by water quench. After that these specimens were cold rolled: 34.4, 41.2, 50 and 72.7%. The cold rolling was carried out in a direction transversal to the original hot rolled direction. These specimens were annealed in a salt pot at 673 K for different times. The stabilization and the annealing temperature were identical in order to minimize precipitation or precipitate dissolution during recrystallization. Furthermore, at 673 K the recrystallization kinetics was not too quick or slow to be followed and studied[23-26].

The metallographic preparation consisted in electrolytic polishing and anodization with Baker's solution. The volume fraction recrystallized and the area per unit of volume were measured by standard quantitative metallography techniques.

4. Results

In what follows specimens (or data obtained from them) that were deformed 34.4 41.2 50 and 72.7% before recrystallization will be referred to as the "34%", "41%", "50%" and "72%" specimens for brevity.

4.1. Initial microstructure characterization

After stabilization heat treatment at 673 K, before cold deformation, the grain size was 80 μm. Two types of precipitates were found after matrix dissolution and X-ray analysis: orthorhombic Al_6(Fe,Mn) and cubic α-Al(Fe, Mn)Si. The total volume percentage of the precipitates was between 4 and 5% . The large majority of the precipitates was elongated and had an average length between 1-5 μm. With the help of transmission electron microscopy rounded particles with a size in the range of 0.1 to 0.4 μm could also be found. Notice that the stabilization treatment carried out at 673 K before the deformation assures that no precipitation is going to take place during recrystallization.

4.2. Measured data

Tables 1, 2 and 3 show the recrystallized volume fraction (V_V), the interfacial area per unit of volume between recrystallized and deformed regions (S_V), the interfacial area per unit of volume between recrystallized and recrystallized regions (S_{VR}) and the Cahn and Hagel velocity (G_{CH}) against annealing time at 673 K for specimens deformed 34, 41 and 50%, respectively. Data from the specimen deformed 72.7% is not shown because in this case the recrystallization was completed in less than 30 s. The final grain size, mean intercept length, λ, in the 72% specimen was equal to 36 μm. On the other hand the specimens that had the lowest deformation before recrystallization, 34%, did not fully recrystallized. The reaction becomes sluggish after 8vol% recrystallized was reached in 40 s. A volume fraction of 13vol% was reached after 129600 s (36 h). In view of the limited amount of data available for the 34 and 72% speci-

Table 1. Recrystallized volume fraction (V_V), the interfacial area per unit of volume between recrystallized and deformed regions (S_V) against annealing time at 673 K for specimens cold rolled 34% (thickness reduction).

Time (s)	V_V	S_V (mm^2/mm^3)
0	—	—
30	0.05	2.03
40	0.08	2.47
120	0.09	-
15420	0.11	-
129600	0.13	-

Table 2. Recrystallized volume fraction (V_V), the interfacial area per unit of volume between recrystallized and deformed regions (S_V), the interfacial area per unit of volume between recrystallized and recrystallized regions (S_{VR}) and the Cahn and Hagel velocity (G_{CH}) against annealing time at 673 K for specimens cold rolled 41% (thickness reduction). The final grain size, mean intercept length, λ, was equal to 141 μm.

Time (s)	V_V	S_V (mm^2/mm^3)	S_{VR} (mm^2/mm^3)	$G_{CH} \times 10^3$ (mm/s)
0	—	—	—	—
20	0.04	1.56	0.12	2.43
35	0.25	6.22	1.80	1.39
60	0.38	7.89	3.51	0.67
120	0.54	6.99	6.60	0.40
300	0.78	3.97	10.83	0.33
600	0.89	3.41	—	0.11
18000	0.91	3.07	12.68	0.0004

Table 3. Recrystallized volume fraction (V_V), the interfacial area per unit of volume between recrystallized and deformed regions (S_V), the interfacial area per unit of volume between recrystallized and recrystallized regions (S_{VR}) and the Cahn and Hagel velocity (G_{CH}) against annealing time at 673 K for specimens cold rolled 50% (thickness reduction). The final grain size, mean intercept length, λ, was equal to 89 μm.

Time (s)	V_V	S_V (mm^2/mm^3)	S_{VR} (mm^2/mm^3)	$G_{CH} \times 10^3$ (mm/s)
0	—	—	—	—
10	0	0	0	—
20	0.07	2.98	1.26	4.96
32	0.32	8.59	4.76	2.69
40	0.53	8.74	9.29	2.45
60	0.91	2.56	20.57	2.36
10800	0.93	2.53	20.99	0.0013
20520	0.97	—	—	—

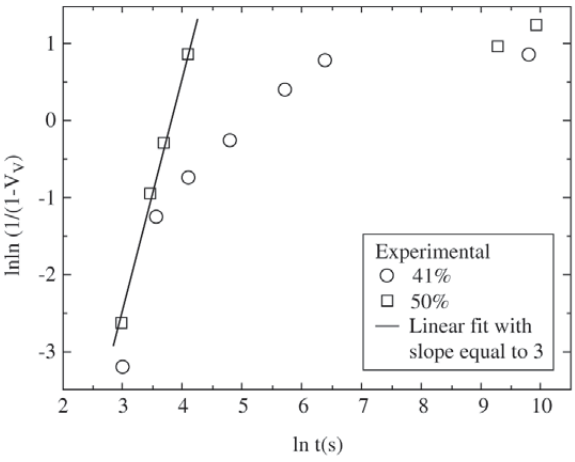

Figure 1. Avrami plot of volume fraction against time data of specimens deformed 41 and 50% and annealed at 673 K. Straight line was best-fitted to 50% experimental data with a fixed slope equal to 3.

mens the following quantitative analysis will concentrate on the 41 and 50% data shown in Tables 2 and 3.

5. Discussion

5.1. Volume fraction against time plot

Figure 1 shows the Avrami plot using data from Tables 2 and 3. A straight line was best-fitted to the 50% experimental data with a fixed slope equal to three. The figure shows that at the initial stages both the 50% and the 41% data follows Eq. 10 with slope equal to three but later in the reaction the slope significantly decreases. This decrease in slope occurs earlier in the 41% specimen. It is not possible to describe the whole kinetics with Eq. 10 with a constant slope equal to n.

5.2. Microstructural path

Tables 2 and 3 show also the area per unit of volume against annealing time at 673 K for specimens deformed 41% and 50%, respectively. Fig. 2 shows the microstructural path plot for the 41 and the 50% specimens. The lines correspond to the microstructural path of site-saturated nucleation, Eq. 15, best-fitted to the experimental data. The parameter "B" defined below was used as a fitting parameter:

$$B = 3\left(\frac{4\pi N_V}{3}\right)^{1/3}$$

The value of B obtained was 18.23 and 21.97 m^{-1} for the 41 and the 50% data, respectively. The agreement between theory and experiment shown in Fig. 2 is good, indicating that the site-saturation assumption describes the experimental data well.

Site-saturation has been frequently observed in aluminum alloys[21,35]. The fact that the microstructural path can be described well by the microstructural path of site-saturated reactions derived above is usually considered to be strong evidence that the recrystallization is indeed site-saturated[28]. This is also related to another question, namely, whether the nucleation can be taken to be random as required by the derivations above. Again it is not easy to give a definite answer to this. But it is not unreasonable to say that this must be at least approximately true since the theory satisfactorily describes the experimental data. Part of the success of these assumptions might even be credited to the significant experimental scatter normally found in recrystallization studies. Second order effects, even if they do exist, need not be considered since the data do not have such a high precision anyway.

5.3. Cahn and Hagel velocity

Tables 2 and 3 show the Cahn and Hagel velocity, G_{CH}, against annealing time at 673 K for specimens deformed 41% and 50%, respectively. Fig. 3 shows the velocity against time plot with data extracted from Tables 2 and 3. Velocities corresponding to annealing times longer than 300 s were left out of Fig. 3. It can be seen that for the 41% specimen G_{CH} decreases continuously. On the other hand for the 50% specimen after an initial drop it remains roughly constant up to an annealing time of 60 s. Examination of Tables 2 and 3 show that in both cases there is a significant drop for longer times. This is in agreement with Fig. 1. The

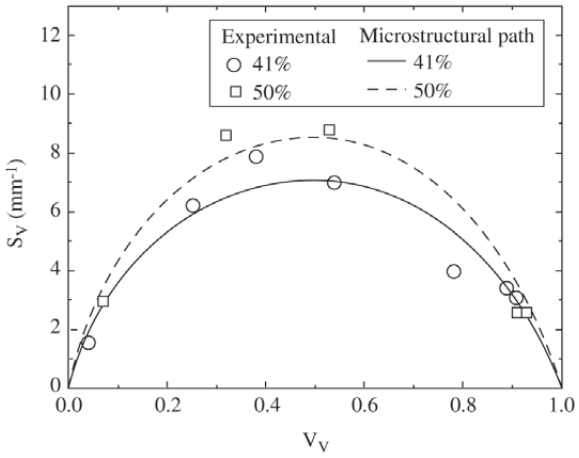

Figure 2. Microstructural path of the specimen deformed 41% and annealed at 673 K. Solid line corresponds to the microstructural path of site-saturated reactions. The agreement between theory and experiment is good, indicating that the site-saturation assumption describes the experimental data well.

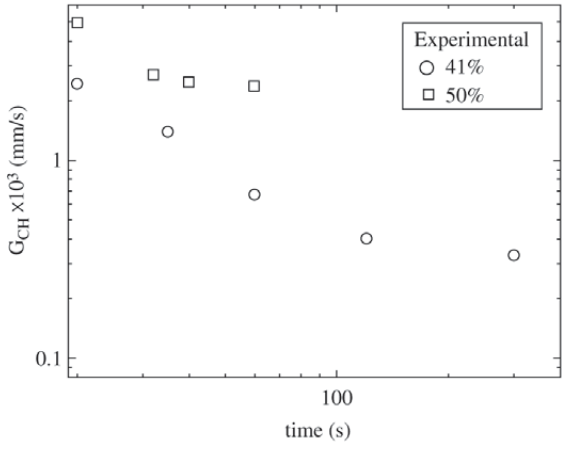

Figure 3. Cahn and Hagel velocity, G_{CH}, against time plot for specimens deformed 41% and 50% and annealed at 673 K. There is a strong decrease in G_{CH} after 60s in the 41% and after 600 s in the 50% specimens. These long time data was left out of the graph due to a scale problem but can be found in Tables 2 and 3.

recrystallization kinetics of the 50% specimen with a slope of three matches a roughly constant G_{CH}.

In section 5.2 it was shown that the recrystallization is site saturated so that the velocity can be directly identified with dR_{ex}/dt, the growth rate of spherical grains in extended space.

It is clear that the velocity decreases with time. As said in the introduction, in single phase alloys this can occur due to two main reasons: a) concurrent recovery and b) stored energy gradients. In the present case Zener drag due to the dispersoids might have played a role, see section 5.6.

5.4. Impingement-compensated chord length

Figure 4 shows the impingement-compensated chord length, λ_{ex}, against annealing time. The solid straight line was best-fitted through zero to the 50% data. In the fitting process only the first four points for annealing times up to 60 s were used. For site-saturated reactions $\lambda_{ex} = 4R_{ex}/3$, so that $d\lambda_{ex}/dt = (4/3)dR_{ex}/dt = (4/3)G_{CH}$. The best-fitted slope gave $d\lambda_{ex}/dt = 0.00491$ mm/s so that $G_{CH} = 3.68 \times 10^{-3}$ mm/s. this agrees well with G_{CH} averaged over the first four points, see Table 3, which gives $\langle G_{CH} \rangle = 3.12 \times 10^{-3}$ mm/s. Concerning the 41% specimens, the plot suggests that after being initially high the velocity decreases but remains approximately constant up to annealing times of 300 s. The dashed straight line in Fig. 4 shows this trend.

5.5. Grain shape considerations for site-saturated recrystallization

Figure 5 shows the plot corresponding to Eq. 24 dis-

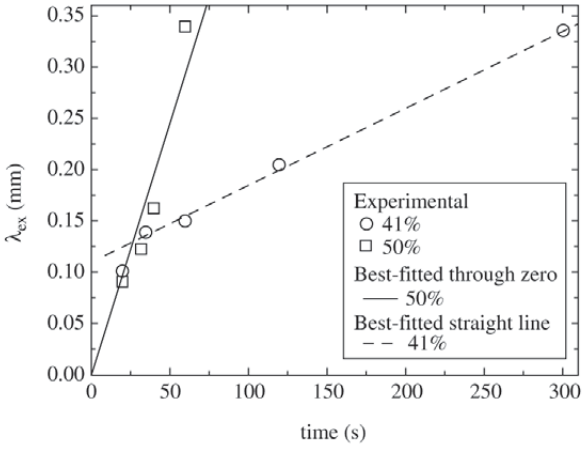

Figure 4. The impingement-compensated chord length, λ_{ex}, plotted against annealing time. Long time data was left out of the graph due to a scale problem but the slope of λ_{ex} decreases for long times matching the decrease in G_{CH} mentioned above.

cussed in section 2.5. Spherical grains should fall close to the $\alpha = 1$ line. It can be seen in Fig. 5 that this is only approximately true in the beginning of the recrystallization. As the volume fraction increases the experimental points increasingly deviate from the $\alpha = 1$ line indicating a strong deviation from the spherical shape. This does not necessarily mean that they do not remain equiaxed. It could mean that their boundaries are becoming "ragged" possibly due

to their interaction with the particles. This is in good agreement with optical microscopy observations, particularly at the end of the recrystallization.

5.6. Effect of particles on the recrystallization in this alloy

As said above, two particle dispersions were found in this alloy: a) 4-5vol% of 1-4 μm; b) 0.1-0.4 μm dispersoids.

These dispersions have an opposite effects. It is well known that[3] a coarse dispersion of hard particles lead to particle stimulated nucleation(PSN). The fine dispersoids could hinder the nucleation demanding a higher deformation to start recrystallization. The nucleation occurs in the region around the coarse particles where there is a very high density of geometrically necessary dislocations. While the nucleus is growing inside this highly deformed zone its velocity is high but it significantly decreases and growth might even stop, as shown by Humphreys and Hatherly[3], when it leaves it. Zener drag caused by the dispersoids as well as recovery could be additional retarding factors to interface migration inside and outside the deformation zone. This high deformation region can be invoked to explain the decrease in grain boundary velocity observed in materials containing large particles. Vandermeer and Jensen[21] used this idea to explain the decrease in grain boundary velocity observed in their commercial AA1050 aluminum alloy. In the present alloy the transformation virtually stops after transforming 9vol% in the 34% specimen, 0.89vol% in the 41% specimen and 0.91vol% in the 50%. In the 72% the transformation proceeds to 100% very fast.

It is natural to make a parallel between the present alloy and the AA1050 studied by Vandermeer and Jensen[21] and explain the decrease in velocity along the same lines, namely, that the recrystallization kinetics in this alloy is a function of the growth of the recrystallized regions nucleated in the deformed zone around the large non-deformable particles present in the microstructure and that the velocity decreases as the interface moves outside this deformation region. However, it is not straightforward to do this. The number of grains per unit of volume can be roughly estimated by $N_V \approx 0.5/\lambda^3$, for $\lambda \approx 100$ μm, $N_V \approx 5 \times 10^2 \approx 10^3$ grains/mm^3. The number of large particles, not including the dispersoids, per unit of volume can be roughly estimated by $N_{VP} \approx 0.24 V_{VP}/r^3$, where V_{VP} and r are the volume fraction and the average particle radius, respectively; for $V_{VP} \approx 0.05$ and $r \approx 1$ μm, $N_{VP} \approx 10^7$ particles/mm^3. The number of particles per unit of volume in the present alloy is several orders of magnitude larger than the number of grains per unit of volume. In these circumstances one cannot identify each particle with a nucleus. Since it is likely that there are high deformation regions around every large particle a more complicated picture of recrystallization emerges in this alloy than in the AA1050.

In conclusion whereas the presence and probably the influence of deformation gradients cannot be denied in this alloy the correlation of the high deformation zones around the particles with the decrease in the grain boundary velocity is not so straightforward. This is so because if PSN is the nucleation mechanism in this alloy the nucleation takes place only at a small fraction of the particles. Other retarding effects such as Zener drag due to the dispersoids and concurrent recovery cannot be ruled out.

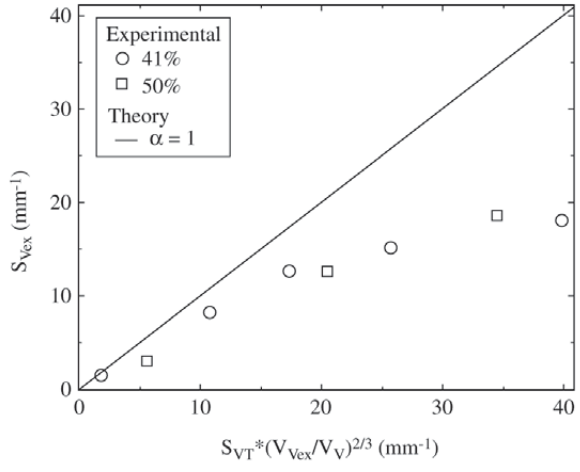

Figure 5. Plot showing the deviation of the grains from spherical shape, possibly developing "ragged" boundaries as a result of particle/boundary interaction.

6. Conclusions

The microstructural path analysis was consistent with site-saturated nucleation in this alloy. As a result, the change in the slope of the volume fraction against time plot was due to a decrease in the grain boundary velocity. This decrease could be seen either in the Cahn and Hagel velocity against time and in the impingement compensated chord length against time plot. This latter quantity was calculated by the new Eq. 18 that was used here for the first time. The analysis also suggested that as the transformation progressed the recrystallized grains significantly deviated from spherical shape. This was attributed to them developing ragged boundaries because of the boundary/particle interaction. As to the effect of particles it is tentatively proposed that whereas the presence and probably the influence of deformation gradients associated with large particles cannot be denied in this alloy the correlation of the high deformation zones around the particles with the decrease in the grain boundary velocity is not so straightforward. This is so because if PSN is the nucleation mechanism in this alloy the nucleation takes place only at a small fraction of the parti-

cles. Other retarding effects such as Zener drag due to the dispersoids and concurrent recovery cannot be ruled out.

Acknowledgements

The authors are grateful to Conselho Nacional de Desenvolvimento Científico e Tecnológico, CNPq, to Fundação de Amparo à Pesquisa do Estado do Rio de Janeiro, FAPERJ, (Research grant E-26/152397/2002, P.R. Rios), and to Fundação de Amparo à Pesquisa do Estado de São Paulo, FAPESP, (Contracts 99/10796-8, Thematic Project, and 01/10134-7, Visiting Professor Scholarship to P.R. Rios).

References

1. Burgers, W.G. *Rekristallisation, verformter Zustand und Erholung*, Akademischer Verlagsgesellschaft, Leipzig, 1941.
2. Haessner, F. (Ed.) *Recrystallization of Metallic Materials*, Dr. Riederer-Verlag GmbH, Stuttgart, 1978.
3. Humphreys, F.J.; Hatherly, M. *Recrystallization and Related Annealing Phenomena*, Pergamon, Oxford, 1996.
4. Beck, P.A.; Sperry, P.R. *Journal of Applied Physics*, v. 21, p. 150-152, 1950.
5. Bailey, J. E. *Philosophical Magazine*, v. 5, p. 485-497, 1960.
6. Bailey, J.E.; Hirsch, P.B. *Proceedings of The Royal Society (London)*, v. 267, p. 11-30, 1962.
7. Cahn, R.W. *Proceedings of the Physical Society of London*, v. 63 (4A), p. 323-336, 1950.
8. Beck, P.A. *Journal of Applied Phisics*, v. 20, p. 633-634, 1949.
9. Smith, C.S. Discussion on paper by Bowles and Boas. *Journal of The Institute of Metals*, v. 74, p. 742-758, 1947/48.
10. Hu, H. in *Recovery and Recrystallization in Metals*, Himmel, L. (Ed), p. 311-362, Interscience Pub., New York, 1963.
11. Hu, H. in *Electron Microscopy and Strength of Crystals*, Thomas, G; Washburn, J. (Eds), p. 564-573, Interscience Pub., New York, 1963.
12. Doherty, R.D.; Szpunar, J.A. *Acta Metallurgica*, v. 32, p. 1789-1798, 1984.
13. Johnson, W.A.; Mehl, R.F. *Transactions AIME*, v. 135, p. 416-441,1939.
14. Avrami, M.J. *Journal of Chemical Physics*, v. 7, p. 1103-1112 , 1939.
15. Avrami, M.J. *Journal of Chemical Physics*, v. 8, p. 212-224 , 1940.
16. Avrami, M.J. *Journal of Chemical Physics*, v. 9, p. 177-184 , 1941.
17. Kolmogorov, A.N. *Izv. Akad. Nauk. USSR-Ser. Matemat*., v. 1. p. 355-359, 1937.
18. DeHoff, R.T. in *Annealing Processes – Recovery, Recrystallization and Grain Growth*, Proceedings, Hansen, N.; Juul Jensen, D.; Leffers, T.; Ralph, B. (Eds), p.35-52, Risø National Laboratory, Roskilde, Denmark, 1986.
19. Vandermeer, R.A.; Masumura, R.A. *Acta metall. mater.*, v. 40, p. 877-886, 1992.
20. Vandermeer, R.A.; Juul Jensen, D. *Interface Science*, v. 6, p. 95-104, 1998.
21. Vandermeer, R.A.; Juul Jensen, D. *Acta Materialia*, v. 49, p. 2083-2094, 2001.
22. Diaz-Mora, N.; Zanotto, E.D.; Hergert, R.; Muller, R. *Journal of Non-Crystalline Solids*, v. 273, p. 81-93, 2000.
23. Ness, E. *Acta Metallurgica*, v.24, p. 391-398, 1976.
24. Furrer, P.; Hausch, G. *Metal Science*, v. 13, p. 155-162, 1979.
25. Lloyd, D.J. *Metal Science*, v. 16, p. 304-308, 1982.
26. Pimenta Jr, F.C.; Arruda, A.C.F.; Padilha, A.F. *Zeitschrift für Metallkunde*, v. 77, p. 522-528, 1986.
27. Cahn, J.W. *Acta Metallurgica*, v. 4, p.449-459, 1956.
28. Vandermeer, R.A.; Rath, B.B. *Metallurgical Transactions A*, v. 20A, p. 391-401, 1989.
29. Speich, G.R.; Fisher, R.M.: *Recrystallization, Grain Growth and Textures*, ASM, Metals Park, OH, p. 563-598, 1966.
30. Stüwe, H-P.; Padilha, A.F.; Siciliano Jr., F. *Materials Science and Engineering A*, v. A233, p. 361-367, 2002.
31. Rios, P.R. *Metallurgical and Materials Transactions A*, v. 28, p. 939-946, 1997.
32. Cahn, J.W.; Hagel, W. *Decomposition of Austenite by Diffusional Processes*, Zackay, Z.D. and Aaronson, H.I. (Eds), Interscience Pub., New York, NY, p. 131-196, 1960.
33. Rios, P.R.; Padilha, A.F. *Scripta Materialia*, v. 48, p. 1561-1564, 2003.
34. Yamamoto T.; Sakuma T.; Rios P. R. *Scripta Materialia*, v. 39, p. 1713-1717, 1998.
35. Vandermeer, R. A. and Gordon, P. *Transactions TMS-AIME,* v.215, p. 577-588, 1959.